Engineering Notes

ENGINEERING NOTES are short manuscripts describing new developments or important results of a preliminary nature. These Notes cannot exceed 6 manuscript pages and 3 figures; a page of text may be substituted for a figure and vice versa. After informal review by the editors, they may be published within a few months of the date of receipt. Style requirements are the same as for regular contributions (see inside back cover).

Inviscid Laval-Nozzle Flowfield Calculation

Stefan Riedelbauch* and Claus Weiland†
Messerschmitt-Bölkow-Blohm GmbH, Munich, Federal Republic of Germany

Introduction

PROPULSION systems for space missions often use Laval nozzles. Therefore a knowledge of the flowfield in such nozzles and its dependence on the nozzle shape and on the fluid is of great importance for the design. Assuming that the influence of the viscous shear layer on the wall is negligible, Euler equations can be employed to determine the inviscid flowfield. Here the equations are used in a quasiconservative formulation. The discretization is based on an upwind finite-difference approximation with characteristic-type boundary conditions. For the simulations, a perfect gas with constant specific heat coefficients is assumed. Two cases with different isentropic exponents, $\gamma = 1.4$ and $\gamma = 1.17$, will be discussed for the same geometry and boundary conditions.

Governing Equations

For axisymmetric fluid flow, the time-dependent Euler equations with general transformation relations in cylindrical coordinates and velocity components

$$\xi = \xi(x, y), \qquad \eta = \eta(x, y), \qquad \tau = t$$

read[1,2]

$$\frac{\partial Y}{\partial \tau} + J\frac{\partial Y}{\partial \xi} + K\frac{\partial Y}{\partial \eta} + H = 0 \tag{1}$$

where the conservative variables are $Y = (\rho, \rho u, \rho v, e)^T$ and the curvature term is $H^T = (\rho v, \rho uv, \rho v^2, (e + p)v)/y$. The matrices J and K are determined by $J = MAM^{-1}$ and $K = MBM^{-1}$,[1,2] where A and B are the Jacobians of the nonconservative Euler equations with dependent variables ρ, u, v, and p.

$$M = \begin{bmatrix} 1 & 0 & 0 & 0 \\ u & \rho & 0 & 0 \\ v & 0 & \rho & 0 \\ \dfrac{u^2+v^2}{2} & \rho u & \rho v & \dfrac{1}{\gamma - 1} \end{bmatrix}$$

$$A = \begin{bmatrix} U & \xi_x \rho & \xi_y \rho & 0 \\ 0 & U & 0 & \xi_x/\rho \\ 0 & 0 & U & \xi_y/\rho \\ 0 & \xi_x \rho c^2 & \xi_y \rho c^2 & U \end{bmatrix} \tag{2}$$

Received Sept. 4, 1986; revision received Oct. 22, 1986.

*Scientist.
†Head of Fluid Dynamics Branch, MBB Space Group.

Matrix B is obtained from A by substituting $U \to V$, $\xi_x \to \eta_x$, and $\xi_y \to \eta_y$. In these expressions, ρ and p are density and pressure, respectively. The variables u and v are the velocity, components in the streamwise (x) and radial (y) directions for cylindrical coordinates. The total energy per volume is defined by $e = p/(\gamma - 1) + \rho(u^2 + v^2)/2$, and c is the speed of sound. The contravariant velocities U and V are given by $U = \xi_x u + \xi_y v$ and $V = \eta_x u + \eta_y v$. As explained, e.g., in Refs. 1, 3, and 4, the matrices A and B can be diagonalized and then split according to the positive and negative eigenvalues, and so can J and K.

$$A = T_A \Lambda_A T_A^{-1} \qquad B = T_B \Lambda_B T_B^{-1} \tag{3}$$

When the matrices are split, Eq. (1) reads

$$\frac{\partial Y}{\partial \tau} + J^+\left(\frac{\partial Y}{\partial \xi}\right)^+ + J^-\left(\frac{\partial Y}{\partial \xi}\right)^- + K^+\left(\frac{\partial Y}{\partial \eta}\right)^+ + K^-\left(\frac{\partial Y}{\partial \eta}\right)^- + H = 0 \tag{4}$$

with

$$J^+ = Q_A \Lambda_A^+ Q_A^{-1} \quad \text{and} \quad Q_A = MT_A$$

According to the theory of characteristics, the sign of the eigenvalues gives insight into the signal propagation. The discretization is accordingly selected in an upwind manner.

Numerical Algorithm

The algorithm applied in the present work is a one-step explicit upwind scheme of first-order accuracy in time and second-order accuracy in space.

$$Y^{n+1} = Y^n + \Delta\tau\left(\frac{\partial Y}{\partial \tau}\right)^n$$

$$\left(\frac{\partial Y}{\partial \tau}\right)^n = -\left[J^+\left(\frac{\partial Y}{\partial \xi}\right)^+ + J^-\left(\frac{\partial Y}{\partial \xi}\right)^- + K^+\left(\frac{\partial Y}{\partial \eta}\right)^+ + K^-\left(\frac{\partial Y}{\partial \eta}\right)^- + H\right]^n$$

$$\left(\frac{\partial Y}{\partial \xi}\right)_m^+ = (3Y_m - 4Y_{m-1} + Y_{m-2})/2\Delta\xi$$

$$\left(\frac{\partial Y}{\partial \xi}\right)_m^- = -(3Y_m - 4Y_{m+1} + Y_{m+2})/2\Delta\xi \tag{5}$$

Similar expressions are used for the η derivatives.

Boundary Conditions

The nozzle contour is mapped onto a ξ = constant coordinate line. Therefore the contravariant velocity U is prescribed by $U = \xi_x u + \xi_y v = 0$. The details of the algorithm are described in Refs. 1 and 2. For the inflow and outflow boundary conditions, the quasiconservative, locally one-dimensional,

characteristic boundary conditions are derived. Suppose these boundaries are lines η = constant; then Eq. (1) becomes[2,3]

$$Q_B^{-1}\frac{\partial Y}{\partial \tau}+\Lambda_B Q_B^{-1}\frac{\partial Y}{\partial \eta}+\underbrace{Q_B^{-1}J\frac{\partial Y}{\partial \xi}+Q_B^{-1}\cdot H}_{R}=0 \qquad (6)$$

Let Q_B^{-1} with $Q_B = MT_B$ be constant, denoted by the lower index o, and R be neglected as usual; then

$$\frac{\partial (Q_{B_o}^{-1}Y)}{\partial \tau}+\Lambda_B\frac{\partial (Q_{B_o}^{-1}Y)}{\partial \eta}=\frac{\mathrm{d}(Q_{B_o}^{-1}Y)}{\mathrm{d}\tau}=0 \qquad (7)$$

where

$$q_1=\left[1-\frac{\gamma-1}{2c_o^2}(u_o^2+v_o^2)\right]\cdot\rho+\frac{u_o(\gamma-1)}{c_o^2}\rho u+\frac{v_o(\gamma-1)}{c_o^2}\rho v-\frac{(\gamma-1)}{c_o^2}e$$

$$q_2=\left(-\sqrt{2}\tilde{\eta}_y\frac{u_o}{\rho_o}+\sqrt{2}\eta_x\frac{v_o}{\rho_o}\right)\rho+\frac{\sqrt{2}\tilde{\eta}_y}{\rho_o}\rho u-\frac{\sqrt{2}\tilde{\eta}_x}{\rho_o}\rho v$$

$$q_3=\left[-\tilde{\eta}_x\frac{u_o}{\rho_o}-\tilde{\eta}_y\frac{v_o}{\rho_o}+\frac{\gamma-1}{2\sqrt{2}\rho_o c_o}(u_o^2+v_o^2)\right]\rho+\left(\frac{\tilde{\eta}_x}{\rho_o}-\frac{(\gamma-1)u_o}{\sqrt{2}\rho_o c_o}\right)\rho u+\left(\frac{\tilde{\eta}_y}{\rho_o}-\frac{(\gamma-1)v_o}{\sqrt{2}\rho_o c_o}\right)\rho v+\frac{\gamma-1}{\sqrt{2}\rho_o c_o}e$$

$$q_4=\left[\tilde{\eta}_x\frac{u_o}{\rho_o}+\tilde{\eta}_y\frac{v_o}{\rho_o}+\frac{(\gamma-1)}{2\sqrt{2}\rho_o c_o}(u_o^2+v_o^2)\right]\rho+\left[-\frac{\tilde{\eta}_x}{\rho_o}-\frac{(\gamma-1)u_o}{\sqrt{2}\rho_o c_o}\right]\rho u+\left[-\frac{\tilde{\eta}_y}{\rho_o}-\frac{(\gamma-1)v_o}{\sqrt{2}\rho_o c_o}\right]\rho v+\frac{\gamma-1}{\sqrt{2}\rho_o c_o}e$$

$$\tilde{\eta}_x=\frac{\eta_x}{\sqrt{2(\eta_x^2+\eta_y^2)}},\qquad \tilde{\eta}_y=\frac{\eta_y}{\sqrt{2(\eta_x^2+\eta_y^2)}}$$

Using Eqs. (2) and (3) and defining $M_o^{-1}Y = X$, one gets

$$\frac{\mathrm{d}(Q_{B_o}^{-1}Y)}{\mathrm{d}\tau}=\frac{\mathrm{d}(T_{B_o}^{-1}M_o^{-1}Y)}{\mathrm{d}\tau}=\frac{\mathrm{d}(T_{B_o}^{-1}X)}{\mathrm{d}\tau}=0 \qquad (8)$$

Equation (8) is formally identical with the nonconservative boundary condition,[1,3] but $X^T = \{\rho,\ (u-u_o)\rho/\rho_o,\ (v-v_o)\rho/\rho_o,\ (\gamma-1)[(u-u_o)^2+(v-v_o)^2]\rho/2+p\}$. Each eigenvalue is associated with a characteristic variable $(Q_B^{-1}Y)$. The sign of the eigenvalue determines the direction of the signal propagation across the computational boundary η = constant. At subsonic inflow, the eigenvalues λ_1, λ_2, and λ_3 are positive, indicating that three variables have to be prescribed, and λ_4 is negative, requiring information from inside the computational domain. Equation (8) yields

$$[q_1]_\infty=[q_1]_B \qquad [q_3]_\infty=[q_3]_B$$
$$[q_2]_\infty=[q_2]_B \qquad [q_4]_I=[q_4]_B \qquad (9)$$

The subscript notation ∞ is for freestream conditions, B for boundary, and I for inside the computational domain.

Using the given one-dimensional theory, the freestream conditions depend on the area ratio of inflow to throat cross section. The expressions in Eq. (9) are expected to give good results in the case of homogeneous flow at the inflow boundary due to the assumption of one-dimensional flow. Therefore a cylindrical tube is added right in front of the actual nozzle (Fig. 1). At the outflow boundary the flow is supersonic and all eigenvalues are positive, so none of the variables needs to be prescribed; therefore a simple three-point extrapolation is used. The three-point extrapolation is better than the two-point extrapolation for maintaining the mass flow and determining the thrust across the cross section. At the symmetry line, symmetric conditions are applied.

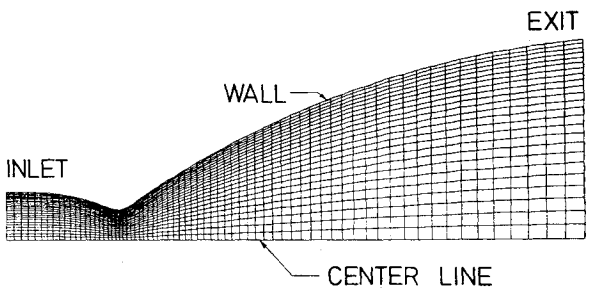

Fig. 1 Computational grid (25 × 71).

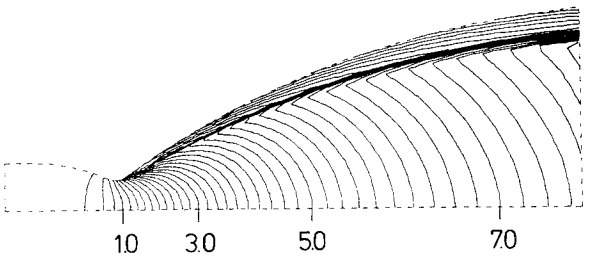

Fig. 2a Mach number ($\gamma = 1.4$).

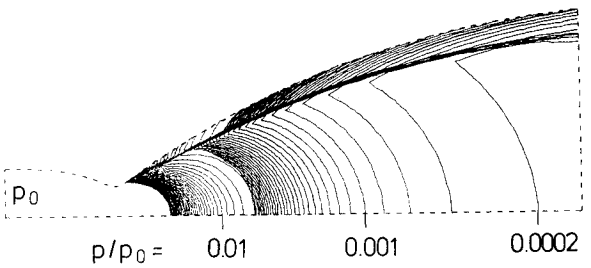

Fig. 2b Static pressure contours ($\gamma = 1.4$).

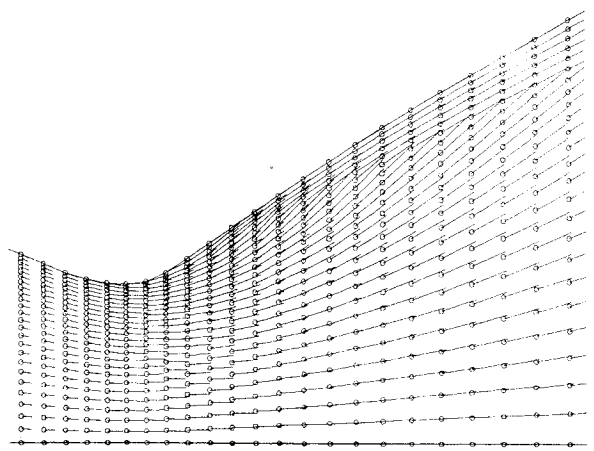

Fig. 2c Velocity vectors near the throat ($\gamma = 1.4$).

Results

Because of the large temperature and pressure differences between the combustion chamber and nozzle exit, the isentropic exponent of the fluid changes considerably. Therefore two results, both at the operation point of the nozzle, are presented for rather different isentropic exponents, one for $\gamma = 1.4$

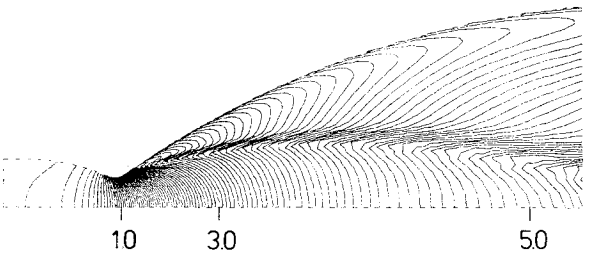

Fig. 3a Mach number ($\gamma = 1.7$).

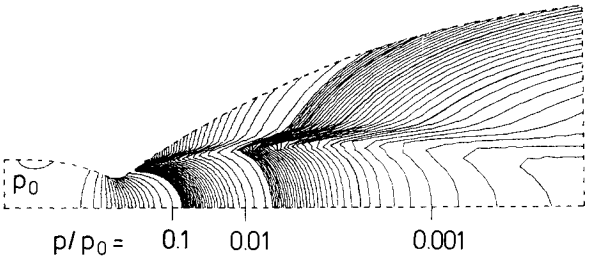

Fig. 3b Static pressure contours ($\gamma = 1.7$).

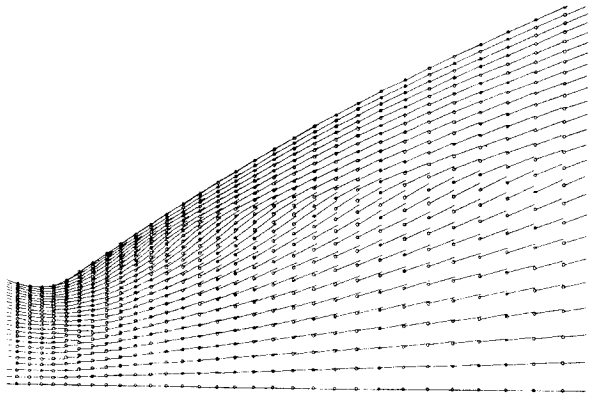

Fig. 3c Velocity vectors near the throat ($\gamma = 1.7$).

and one for $\gamma = 1.17$, using the same geometry. Figure 1 shows the 25×71 grid. The coordinate lines are concentrated in the wall region and near the throat, where large flow gradients are expected. Figures 2a–c show the lines of constant Mach number, the pressure, and the velocity vectors near the throat for the $\gamma = 1.4$ case. A shock wave is observed in the expansion part of the nozzle close to the wall and nearly parallel to it. The maximum exit mach number is about 8.2. The pressure varies about a factor of 500 from the nozzle inlet to exit. This does not cause any difficulties for the applied algorithm during the transient phase. Note that Fig. 2b (see also Fig. 3b) has been obtained by subdividing the nozzle in the axial direction into two (three) domains for the graphics. In each region, a different increment was used for the plot of the isobars to cope with the large axial pressure differences without creating large black or white regions. For the $\gamma = 1.7$ case, Figs. 3a–c show the Mach number, pressure contours, and velocity vectors respectively. Again a shock wave occurs. This shock wave is significantly weaker than for $\gamma = 1.4$, and its location and shape differ considerably from those of the former flow. Here the maximum exit Mach number is about 5.3, and the pressure ratio is roughly 200. The comparison of the two flows shows a large difference in inviscid flow structure due to the different isentropic exponents.

References

[1]Weiland, C., "A Split-Matrix Method for the Integration of the Quasi-Conservative Euler-Equations," Notes on Numerical Fluid-Mechanics, *Proceedings of the Sixth GAMM-Conference on Numerical Methods in Fluid Mechanics*, Vol. 13, Vieweg Verlag, 1986, pp. 383–390.

[2]Riedelbauch, S., "Berechnungen von Düsenströmungen," Diplomarbeit erschienen an der Technischen Universität München, Lehrstuhl für Strömungsmechanik, Berichtsnr. 86/6, 1986.

[3]Whitfield, D. L. and Janus, J. M., "Three-Dimensional Unsteady Euler-Equations Solution Using Flux Vector Splitting," AIAA Paper 84-1551, 1984.

[4]Chakravarthy, S. R., Anderson, D. A., and Salas, M. D., "The Split-Coefficient Matrix Method for Hyperbolic Systems of Gas Dynamic Equations," AIAA Paper 80-0268, 1980.

Rule for Optimizing the Performance of Canted, Scarfed Nozzles

Robert L. Glick*
Talley Defense Systems, Mesa, Arizona
and
Jay S. Lilley†
U.S. Army Missile Command
Redstone Arsenal, Alabama

Nomenclature

A	= area
C_F	= thrust coefficient
F	= thrust
$\dot{m}$	= mass-flow rate
M	= Mach number
p	= pressure
r	= radius
u	= velocity
δ	= cant angle
Γ	= gas dynamic constant
γ	= specific heat ratio
θ	= scarf angle
ρ	= density
ξ	$= 1 - \tan\theta\tan\delta$

Subscripts

a	= atmospheric
c	= chamber
e	= exit
opt	= optimum
s	= component normal to nozzle axis
t	= throat
v	= component along missile's axis

Introduction

IN several applications of importance to rocket propulsion (tandem motors, thrust reversers, aft guidance links), the propulsive nozzle cannot be colinear with the vehicle's axis, and canted, scarfed nozzles must be employed. There are two basic approaches to predicting the performance of these nozzles: numerical integration of the equations of motion for realistic geometry and flowfield conditions[1,2] or simplification of flowfield and geometry to permit a "closed form" solution.[3] Justification for the latter approach is simplicity and the clear revelation of governing physical principals.

Received Nov. 10, 1986. This paper is declared a work of the U.S. Government and is not subject to copyright protection in the United States.

*Principal Engineer. Associate Fellow AIAA.
†Aerospace Engineer, Propulsion Directorate. Member AIAA.